Computers and Geotechnics 106 (2019) 205–216

Contents lists available at ScienceDirect

Computers and Geotechnics

journal homepage: www.elsevier.com/locate/compgeo

Research Paper

Probabilistic analysis of an offshore monopile foundation taking into account the soil spatial variability

Abdul-Kader El Haj[a,*], Abdul-Hamid Soubra[a,*], Jamal Fajoui[b]

[a] University of Nantes, Bd. de l'Université, 44603 Saint-Nazaire Cedex, France
[b] University of Nantes, 58 Rue Michel Ange, 44606 Saint-Nazaire Cedex, France

ARTICLE INFO

Keywords:
Monopile
Probabilistic analysis
Kriging
Failure probability

ABSTRACT

Numerical 3D deterministic models of offshore monopile foundations are computationally-expensive and thus they present a great obstacle to the use of the conventional Monte Carlo Simulation (MCS) methodology for the probabilistic analysis. In this paper, a reliable and efficient Kriging-based probabilistic model called Global Sensitivity Analysis enhanced Surrogate (GSAS) modeling is used. The objective is to perform a probabilistic analysis of a monopile foundation subjected to a combined loading. An undrained normally consolidated clayey soil with spatially varying soil properties was considered. Some probabilistic numerical results are presented and discussed.

1. Introduction

The probabilistic approaches allow one to rigorously take into account the uncertainties of the soil properties and the spatial variability of these properties. The outcomes of these approaches may be the statistical moments of the system response or the probability of failure against an acceptable threshold of this system response. For the probabilistic analyses of offshore geotechnical structures, one may cite among others [1,2] for the bearing capacity of spudcan foundations [3], for the bearing capacity of skirted foundations [4], for the bearing capacity of a gravity-based foundation and [5], for the problem of a monopile foundation. In this paper, a probabilistic analysis of an offshore monopile foundation subjected to a combined loading was investigated. The objective is the computation of the failure probability against exceeding a prescribed threshold of the system response. An undrained normally consolidated clayey soil with spatially varying soil properties was considered in the analysis.

As is well known, the numerical 3D deterministic models of offshore monopile foundations are very time consuming because they are based on finite element/finite difference methods. For this reason, the computation of the failure probability P_f of these structures by the conventional Monte Carlo Simulation (MCS) methodology is unaffordable especially when computing the small practical values of the failure probability in the order of 10^{-3}–10^{-4}. Indeed, one million of calls to the mechanical model are required for the computation of P_f value in the order of 10^{-4} for a coefficient of variation on P_f of 10%.

In order to overcome the shortcoming of the large number of calls to the mechanical model required by MCS methodology, some authors have resorted to more advanced simulation methods called 'variance reduction techniques' such as subset simulation (SS) or asymptotic sampling (AS) [5–12]. Although the variance reduction techniques are powerful probabilistic approaches, they remain insufficient when dealing with a small value of the failure probability and a small desired value of the coefficient of variation on this failure probability. Consequently, more advanced probabilistic approaches requiring a smaller number of calls to the mechanical model are needed.

In the past few years, some probabilistic approaches based on metamodeling techniques have gained a lot of interest. These approaches consist in replacing the time consuming mechanical model by a metamodel (i.e. an analytical equation) making use of a much smaller number of calls to the computationally expensive mechanical model as compared to the crude MCS methodology. The computation of the failure probability by these methods is thus performed by applying MCS methodology on the obtained metamodel with a quasi-negligible computation time. It should be emphasized here that when computing the failure probability by the metamodeling approaches, a small value of the coefficient of variation on the failure probability can be obtained since the huge number of calls of the mechanical model required by MCS is not an issue in this case; the computation time of the system response *via* the metamodel being negligible.

Recently, two kriging-based metamodeling approaches called Active learning methods combining Kriging and MCS [or IS (Importance

* Corresponding authors.
E-mail addresses: abdul-kader.el-haj@etu.univ-nantes.fr (A.-K. El Haj), Abed.Soubra@univ-nantes.fr (A.-H. Soubra), Jamal.Fajoui@univ-nantes.fr (J. Fajoui).

https://doi.org/10.1016/j.compgeo.2018.10.011
Received 24 May 2018; Received in revised form 17 October 2018; Accepted 17 October 2018

Sampling)] have been developed [13,14]. These methods are named AK-MCS and AK-IS respectively. They were shown to be efficient with respect to the classical crude MCS methodology as one can obtain an accurate probability of failure needing a smaller number of calls to the mechanical model. Notice however that the essential issues in these approaches are (i) the choice of a best new training sample for the construction of the metamodel and (ii) the stopping criterion related to the addition of a new training sample. Indeed, these issues are defined from the perspective of individual responses. This may lead to some extra evaluations of unnecessary added training samples. In order to overcome these shortcomings, a Global Sensitivity Analysis enhanced Surrogate (GSAS) modeling was recently developed by Hu and Mahadevan [15]. Within GSAS, a powerful stopping criterion was suggested and a new way of selecting a next training sample was proposed. The new training samples are identified according to their contribution to the uncertainty in the reliability estimate and the addition of training samples stops when the accuracy of the reliability estimate reaches a specific target.

It should be mentioned that Hu and Mahadevan [15] have validated their method based on several academic examples where the performance function was given by an analytical equation. The aim of this paper is to extend the GSAS approach proposed by Hu and Mahadevan [15] to the case of random field problems in order to study geotechnical structures involving spatial variability of the soil properties. More specifically, this paper presents a probabilistic analysis at the Serviceability Limit State SLS of a large diameter monopile foundation embedded in a spatially varying clay and subjected to a prescribed combined loading. The objective is the computation of the failure probability against exceeding a threshold value on the monopile head rotation. Notice that the soil undrained cohesion and the soil undrained Young modulus were considered as random fields. The Expansion Optimal Linear Estimation (EOLE) method proposed by [16] was used to generate the random fields. The mechanical model employed to calculate the system response (i.e. the monopile head rotation) was based on numerical simulations using Abaqus finite-element software.

This paper is organized as follows: The next section presents the mechanical model. This is followed by an overview on the modeling of the soil spatial variability. Then, the coupled mechanical probabilistic model based on GSAS approach (as applied to the case of a large diameter monopile embedded in a spatially varying clayey soil) is described. Finally, some numerical probabilistic results are presented and discussed. The paper ends by a conclusion of the main findings.

2. Mechanical model for the soil-monopile system

A 3D finite element model of the soil-monopile system has been carried out using the commercial software Abaqus/Standard [17].

Table 1 provides the geometrical and material properties of the monopile. An open-ended steel monopile of 3 m diameter was considered in this study. The wall thickness of the monopile was taken equal to 5 cm, thus respecting the following minimum wall thickness provided by API (2000) [18]:

$$t = 6.35 + \frac{D}{100} \quad (1)$$

where t[mm] is the wall thickness of the monopile and D[mm] its outer diameter. The embedded length of the monopile, L, was taken equal to 18 m. The monopile was extended of 1.0 m above the seabed to prevent the soil from going over the monopile [19]. The slenderness ratio L/D is equal to 6 in this paper thus respecting the slenderness ratio corresponding to large diameter offshore monopiles with rigid behavior (L/D < 10 according to [20] and 5 < L/D < 6 according to [21,22]). The steel monopile material with a density of 7840 kg/m^3 was assumed to be linear elastic with Young's modulus E_p of 210 GPa and Poisson's ratio ν_p of 0.3. Concerning the type of soil used in the numerical simulations, an undrained normally consolidated clay with a mean undrained cohesion value of 50 kPa and a mean undrained Young modulus value of 10 MPa was considered in the analysis. The soil was assumed to follow the elastic-perfectly plastic Tresca constitutive model which is defined by the undrained cohesion c_u, the undrained Young's modulus E_u and the Poisson's ratio ν_u. In this paper, the soil was assumed to have a saturated unit weight of 18 kN/m^3 and a Poisson ratio of 0.495. The soil undrained cohesion was considered as a random field. Only the vertical soil variability was considered in the analysis. The soil undrained Young modulus was assumed to be linearly related to the soil undrained cohesion such that $E_u = K_c \times c_u$ where K_c was taken equal to 200 in this work (see [23]). Thus, the soil Young modulus was implicitly considered as a random field having the same distribution as the soil undrained cohesion. Notice that K_c is a correlation factor that is dependent on the clay plasticity index and the over-consolidation ratio OCR [24]. The statistical input data of the soil undrained cohesion will be given later in this paper when dealing with the numerical results.

An offshore monopile that is subjected to a vertical load V (representing the structure weight) together with a horizontal force H acting at a height h (supposed equal to 38.6 m above the sea bed level) is considered in the analysis. The moment at mudline level is thus M= H× h. In this paper, the vertical and horizontal loads are supposed to be equal to 2 MN and 0.55 MN respectively.

Although an entire soil domain is required while considering the spatial variability in three-dimensions, only one-half of this soil domain is adopted in this paper (see Fig. 1). This is because only the vertical soil variability was taken into account in the analysis. As may be seen from Fig. 1, the numerical model has a diameter of 20D and a height equal to 1.6 L. It was verified that with these model dimensions, the behavior of the soil-monopile system was not influenced by the artificial boundary effects. Concerning the model boundary conditions, the bottom of the soil model was fixed against translation in all directions whereas the lateral cylindrical boundary was fixed against lateral translation. Due to symmetry, the symmetrical vertical plane (i.e. the loading plane) was fixed against translation in its normal direction. The soil mesh was constructed using C3D8 and C3D6 linear brick elements (cf. [25]). Incompatible mode linear brick elements (C3D8I) were used for the monopile in order to accurately simulate its flexural behavior (cf. [25]). An illustration of the adopted mesh is shown in Fig. 1.

Surface-to-surface master/slave contact formulation was used to model the interaction between the monopile and the soil. Since the monopile is much stiffer than the soil, it was selected as the master surface while the soil in contact with the monopile was selected as the slave surface. In order to model the normal behavior, a hard contact relationship (called hard pressure-overclosure relationship) is used with a constraint enforcement method of the linear penalty type. In this method, the normal stiffness is set by default to 10 times the representative underlying element stiffness (cf. [25]). Notice that the "hard" contact relationship minimizes the penetration of the slave surface into the master surface at the constraint locations and it does not allow the transfer of tensile stress across the interface. The surfaces separate if the contact pressure reduces to zero. Concerning the frictional behavior, it was modeled using Coulomb friction law: the

Table 1
Geometrical and material properties of the monopile.

Outer diameter D (m)	Thickness t (m)	Embedded length L (m)	Density (kg/m^3)	Young modulus E_p (GPa)	Poisson ratio ν_p
3.00	0.05	18.00	7840	210	0.3

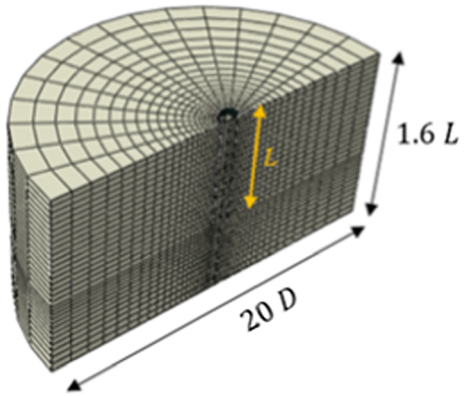

Fig. 1. Soil domain and mesh used in the numerical simulations of the soil-monopile system.

maximum shear stress at contact was equal to the contact stress multiplied by the friction coefficient μ where μ was taken equal to 0.24 in this paper. According to [26], this coefficient was found to lie within the range [0.2–0.4]. This range is in a quite agreement with the values provided by [27,28]. When the shear stress reaches the maximum value, the surfaces slide relative to one another in the tangential direction.

The finite element calculation was executed step-wised. A geostatic step was first performed for the generation of the initial stress state of the soil in the whole model consisting of soil elements only. This is done by defining an isotropic stress field using a coefficient of earth pressure at rest $K_0 = 1$, and then running the geostatic step in the presence of the gravity forces. This leads to a first equilibrium state of the soil mass with negligible deformations. In a second step, the monopile was simulated by (i) removing the soil elements located at the monopile position and generating the steel elements representing the monopile, (ii) activating the contact conditions between the monopile and the soil and (iii) applying the weight of the generated monopile. Finally, in a third step, the horizontal and vertical forces and the corresponding moment are applied in increments at a reference point (taken here at the top of the monopile) where the applied moment was equal to $M = H \times (h - 1) = 20.68$ MN·m.

For an undrained cohesion c_u of 50 kPa and an undrained Young's modulus E_u of 10,000 kPa ($= 200 \times c_u$), the obtained value of the monopile rotation at mud-line is equal to 0.23°. This value is slightly lower than the limit rotation value $\theta_{SLS} = 0.25°$ imposed in this paper at the Serviceability Limit State.

3. Modeling of the soil spatial variability

The spatial variability of the soil properties is an aleatory source of uncertainty resulting from depositional and post-depositional processes. It has significant effects on the reliability of geotechnical structures [29–32]. In order to completely consider its effects, a probabilistic characterization is essential, for which the spatial variability is often identified by the random field theory [33] where it can be described by a probability density function PDF (i.e. mean and standard deviation) and an autocorrelation function with a corresponding value of the autocorrelation distance or the scale of fluctuation. The scale of fluctuation defines the distance beyond which there is not a significant correlation of material property values [34].

Based on some investigations on the variability of seabed soils, Lacasse and Nadim [35] found that the undrained cohesion of clay followed a normal or lognormal distribution with a coefficient of variation ranging between 5% and 35%. According to [1], the scale of fluctuation of offshore soils ranges between 7 m and 9000 m in horizontal direction. In vertical direction, the scale of fluctuation is much smaller, ranging between 0.4 m and 7.14 m. Because of its smaller effect on the computed response, the horizontal variability of the soil was not taken into account in this work.

In this paper, the undrained soil cohesion c_u of the clay was modeled by a lognormal random field Z^{LN} with a square exponential autocorrelation function $\rho_Z^{LN}(X, X')$. This function provides the values of the correlation between two arbitrary points $X(x, y, z)$ and $X'(x', y', z')$ as follows:

$$\rho_Z^{LN}(X, X') = \exp\left[-\left(\frac{|z - z'|}{a_z}\right)^2\right] \quad (2)$$

where a_z is the vertical autocorrelation distance. As may be seen from Eq. (2), only the vertical correlation structure of the soil cohesion was considered in this work. Note that for a square exponential autocorrelation function, the autocorrelation distance a in a given direction is related to the scale of fluctuation δ in that direction by $\delta = \sqrt{\pi}a$.

The EOLE method proposed by Li and Der Kiureghian [16] to discretize a random field was used herein. This method has the advantage that it allows one to determine the variance of the error of the corresponding discretization scheme and thus, it allows one to determine the minimal (optimal) number of eigenmodes for a prescribed value of the variance of the error. EOLE was employed for the generation of the realizations of the cohesion random field, the realizations of the Young modulus random field being obtained by multiplying the cohesion values by 200.

It should be noted that the discretisation of a random field by EOLE leads to an expression that provides the value of this random field at each point of the soil mass as a function of M standard Gaussian random variables (this number M is equal to the number of eigenmodes). For a prescribed value of the variance of the error on EOLE, the number M is small for the high values of the autocorrelation distances (i.e. case of a homogeneous soil) and it becomes significant for the very small values of the autocorrelation distances. For more details on the discretisation of a log-normal random field by EOLE, the reader may refer to Al-Bittar and Soubra [36].

4. Coupled mechanical probabilistic model

The coupled mechanical probabilistic model used to perform the probabilistic analysis may be described by the following steps:

1. After the generation of the random field c_u (and the computation of the random field $E_u = K_c \times c_u$), material random properties values were saved as solution-dependent state variables (SDV) and transmitted to the soil elements by a User defined material subroutine UMAT written in Fortran (see [37] for more details). The objective is to perform an Abaqus numerical simulation (based on the obtained realizations of c_u and E_u) for the computation of the monopile head rotation under the applied combined loading. It should be noted that the UMAT subroutine was used herein to define an elastic-perfectly plastic Mohr-Coulomb constitutive model for the soil behavior that can consider different values of the soil shear strength parameters from element to another one. Indeed, it was not possible to spatially vary the soil shear strength parameters using the Abaqus built-in Mohr-Coulomb constitutive model. A typical realization of the soil cohesion random field is shown in Fig. 2 (notice that SDV4 in Fig. 2 represents the soil undrained cohesion).
2. After each numerical simulation (mechanical calculation) using Abaqus, the post-processing of the mechanical model response was performed using the *Abaqus2Matlab* toolbox [38]. This toolbox is a suitable piece of software which is able to connect Abaqus with Matlab. Using this toolbox, the monopile nodes displacement values at the mud-line level were read in Matlab and then used to compute the monopile rotation value of the corresponding simulation. Finally, the response is stored in Matlab and used by the probabilistic GSAS method presented in the following sub-section.

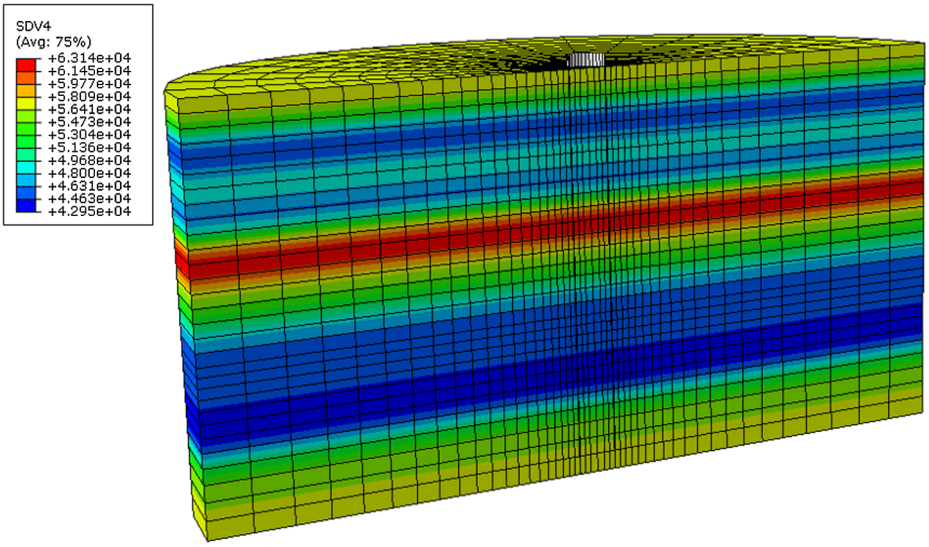

Fig. 2. Typical realization of the soil undrained cohesion.

4.1. GSAS methodology for spatially varying soil problems

GSAS approach is based on the kriging metamodeling theory. The kriging consists in constructing a meta-model (i.e. an analytical model) based on a few number of samples computed using the mechanical model. The predicted response at an unknown sample (based on the constructed kriging meta-model) is a Gaussian random variate characterized by a mean prediction value and a corresponding prediction variance. Details on kriging metamodeling were not provided herein and the reader may refer to [39] or to different recently published papers using kriging metamodeling as in [13,14,40]. It should be emphasized here that contrary to other types of meta-models, the kriging meta-model provides not only a predicted value at an unknown sample but also an estimate of the prediction variance which gives an uncertainty indication on the kriging meta-model at this sample. The variances of the samples used for the construction of the meta-model are zero (i.e. the corresponding predictions are exact), but the variances of the other samples are always different from zero. The construction of a kriging metamodel can be easily performed using DACE (Design and Analysis of Computer Experiments) toolbox in Matlab. For more details, the reader may refer to [41].

The general procedure of the GSAS method (which may be considered as an improvement of AK-MCS by [13]) as adapted to the case of random fields problems can be described by the two following stages (see also the flowchart presented in Fig. 4).

Stage 1: Construction of an approximate kriging meta-model: This stage may be summarized by the following steps:

- Generation by Monte Carlo simulation of $x^{(i)}(i = 1, 2, ...,N_{MCS})$ samples. In this work, N_{MCS} was taken equal to 500,000. Each sample $x^{(i)}$ consists of M standard Gaussian random variables where M is the number of random variables needed by EOLE methodology to accurately discretize the cohesion random field. This number will be given later in this paper [see Table 3].
- Random selection of a small design of experiments DoE from the generated population (a DoE of 15 samples was used in this work). Then, use EOLE methodology to transform each sample into a realization of c_u and a corresponding realization of E_u that provide the spatial distribution of the soil undrained cohesion and Young modulus. For each selected sample, the performance function G is evaluated using the following equation:

$$G = \frac{\theta_{SLS}}{\theta} - 1 \tag{3}$$

where $\theta_{SLS} = 0.25°$ is the limit rotation value considered in this paper and θ is the monopile rotation at mudline computed based on the Abaqus mechanical model making use of the obtained realizations of c_u and E_u.

- Based on the DoE and the corresponding performance function values, construct an approximate kriging meta-model in the standard space of random variables using the DACE toolbox [41]. Remember here that for each Monte Carlo sample $x^{(i)}$, the random response predicted by the approximate kriging surrogate model is a Gaussian variate as follows:

$$G_p(x^{(i)}) \sim N(\hat{g}(x^{(i)}), \sigma^2_{G_p}(x^{(i)})) \tag{4}$$

where G_p is the random response predicted by the kriging metamodel, N stands for the normal distribution and finally $\hat{g}(x^{(i)})$ and $\sigma^2_{G_p}(x^{(i)})$ are the mean prediction and the corresponding mean square error (kriging prediction variance) respectively.

- Determine (for the whole MCS samples) the kriging predictions values $\hat{g}(x^{(i)})$ (i.e. mean values) and their corresponding kriging prediction variance values $\sigma^2_{G_p}(x^{(i)})$ using the DACE toolbox. Then, compute the failure probability $\hat{P}_f$ using the following equation:

$$\hat{P}_f = \sum_{i=1}^{N_{MCS}} I(G_p(x^{(i)})) \Big/ N_{MCS} \tag{5}$$

where the meta-model random responses $G_p(x^{(i)})$ in this equation are replaced by the mean prediction values $\hat{g}(x^{(i)})$. Notice that in Eq. (5), $I(G_p(x^{(i)})) = 1$ if $G_p(x^{(i)}) \leqslant 0$; otherwise, $I(G_p(x^{(i)})) = 0$. Thus, $\hat{P}_f$ is estimated by counting the number of negative mean predictors and dividing it by the total number of MCS samples. The corresponding coefficient of variation $COV(\hat{P}_f)$ is given by the following equation:

$$COV(\hat{P}_f) = \sqrt{\frac{1 - \hat{P}_f}{\hat{P}_f \cdot N_{MCS}}} \tag{6}$$

It should be emphasized here that the value of the failure probability computed at this stage is far from being accurate because of the small DoE used so far. An enrichment process is thus needed.

Stage 2: Enrichment process:

Within AK-MCS approach, the best next candidate sample adopted during the enrichment process is selected as the one that is the most close to the limit state surface. This sample could be considered as the one that mostly reduces the uncertainty in $\hat{P}_f$ if the sample responses

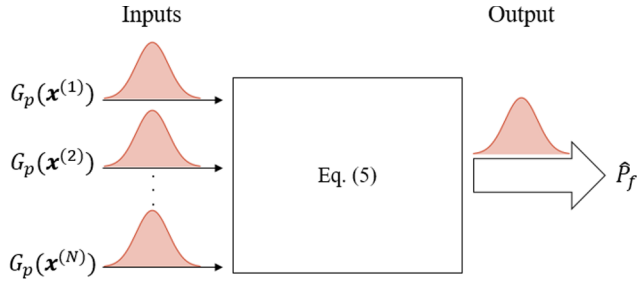

Fig. 3. Probability of failure estimate as a system response (after Hu and Mahadevan [15]).

$G_p(x^{(i)})$ predicted from the surrogate model were completely independent. Notice however that these sample responses are correlated normal variables according to the property of the kriging model. The GSAS approach allows one to overcome this shortcoming as follows.

The basic idea of GSAS is to treat the probability of failure estimate $\widehat{P}_f$ as a random variate representing the output of the system presented in Fig. 3 where the system inputs are the random responses $G_p(x^{(i)})$ predicted by the kriging meta-model. In other words, the uncertainty in the input random variates $G_p(x^{(i)})$ is propagated through the system given by Eq. (5) and thus, the uncertainty in the failure probability estimate can be quantified. Notice that the uncertainty in the failure probability is an epistemic uncertainty since it comes from the uncertainty related to the kriging metamodel predictions. Indeed, this failure probability is calculated based on the responses that are predicted by the constructed kriging metamodel. It should be emphasized that this uncertainty is successively reduced when improving the constructed kriging metamodel during the enrichment procedure.

Finally notice that both the convergence criterion and the strategy of selecting new training samples are defined within GSAS from the perspective of reliability estimate instead of individual responses of MCS samples as will be described in some details in the following subsection.

4.1.1. Choice of the new sample and stopping condition

For an efficient enrichment of the kriging meta-model, the new training sample is selected within GSAS based on its contribution to the uncertainty of the quantity of interest (i.e. $\widehat{P}_f$). It should reduce the uncertainty in $\widehat{P}_f$ in the most significant way. This is done *via* a global sensitivity analysis method extended to the case of models with dependent inputs. The extended FAST method developed by [42] was used in this paper. The enrichment process within GSAS approach can be briefly described as follows:

The MCS samples were firstly classified into two sets according to their U values where U is a learning function usually employed in the kriging-based approaches (cf. [13,14]). It is given by the following equation:

$$U(x^{(i)}) = \frac{|\hat{g}(x^{(i)})|}{\sigma_{G_p}(x^{(i)})} \tag{7}$$

Notice that a large value of U indicates a low probability of making an error on the sign of $\hat{g}(x)$. For $U(x) > 2$, the probability of making a mistake on the sign of the performance function value is < 0.023 (cf. [13]). Based on that, the MCS samples $x^{(i)}(i = 1, 2, ...,N_{MCS})$ are divided into two sets: The first set is composed of the samples with U values that are larger than 2. This set is denoted x_{g1}^{MCS}. The second set includes the remaining samples in $x^{(i)}(i = 1, 2, ...,N_{MCS})$ and it is denoted x_{g2}^{MCS}. Notice that the number of samples in set x_{g1}^{MCS} is denoted in this paper by N_1 and that of the set x_{g2}^{MCS} is denoted by N_2.

The global sensitivity analysis was performed on the samples of the set x_{g2}^{MCS}. The objective is to determine the contribution of each sample of this set to the uncertainty of $\widehat{P}_f$. The reason why the global sensitivity analysis was performed on the set x_{g2}^{MCS} is attributed to the fact that the elements of the set x_{g1}^{MCS} have U values that are larger than 2 and thus, they are likely not contributing to the uncertainty of $\widehat{P}_f$. In order to reduce the dimensionality of the problem, only a reduced number n_{can} of samples (taken equal to 20 in this work) of the set x_{g2}^{MCS} with the lowest U values were selected to perform the global sensitivity analysis. This is because these samples are more likely to have wrong performance function signs (i.e. high probability of being the new selected training sample). Notice that the number $n_{can} = 20$ samples was chosen in this paper for the global sensitivity analysis GSA because a higher number of samples was checked and shown to significantly increase the computation time of the analysis. Indeed, the GSA computation time increases with the increase of n_{can} and it becomes very significant beyond 20 samples in the present problem of monopile foundation. This number of samples was thus adopted for all configurations treated in this paper.

Concerning the stopping condition, a powerful stopping criterion was suggested within GSAS approach. This criterion is based on the quantification of the uncertainty in the failure probability coming from the uncertainty in the responses of the Monte Carlo samples that are predicted by the kriging metamodel. Although a prescribed maximal value of the uncertainty on the failure probability would be a quite relevant stopping condition (because it makes sure that the uncertainty in $\widehat{P}_f$ is sufficiently small), Hu and Mahadevan [15] suggest stopping the addition of new samples based on the uncertainty of the error on the failure probability ε_r. The error on the failure probability is a measure of the gap between the 'theoretical' value and the predicted value of the failure probability. It is defined by the following equation:

$$\varepsilon_r = \frac{\widehat{P}_f - \widehat{P}_f'}{\widehat{P}_f} \tag{8}$$

where $\widehat{P}_f$ is the 'theoretical' failure probability given by Eq. (5) that takes into account the uncertainty in the responses of the set x_{g2}^{MCS} and $\widehat{P}_f'$ is the estimate value of the failure probability computed based on Eq. (5) making use of the kriging meta-model mean prediction values $\hat{g}(x^{(i)})$.

It should be noted here that $\widehat{P}_f$ in Eq. (8) is a random variate for which one can quantify the corresponding uncertainty. This is because $G_p(x^{(i)})$ in Eq. (5) is a Gaussian variate. The uncertainty in ε_r as given by Eq. (8) was thus quantified herein based on the uncertainty quantification of $\widehat{P}_f$. The sampling-based method was used as follows.

The random responses $G_p(x_{g2}^{MCS}(i))$, $i = 1, 2, ...,N_2$ corresponding to the set x_{g2}^{MCS} are correlated normal variables. They are used to generate n_r samples ($n_r = 600$ in this work) of size N_2. From these samples, one can compute n_r samples of the failure probability $\widehat{P}_f$ [using Eq. (5)] and other n_r corresponding samples of the error ε_r [using Eq. (8)]. From the different samples $\varepsilon_r(i)$, $i = 1, 2, ...,n_r$, the Kernel Smoothing function is employed to fit the distribution of the error ε_r. Based on the fitted distribution, Hu and Mahadevan [15] have suggested stopping the addition of new samples when the quantity $\varepsilon_r^{\max}$ becomes smaller than a prescribed threshold t (t is taken equal to 0.1% in this paper) where $\varepsilon_r^{\max}$ is defined as follows:

$$\varepsilon_r^{\max} = \max\{|F_{\varepsilon_r}^{-1}(0.99)|, |F_{\varepsilon_r}^{-1}(0.01)|\} \tag{9}$$

In this equation, $F_{\varepsilon_r}^{-1}$ is the inverse CDF of ε_r. The proposed stopping condition corresponds to a probability of 2% that the estimation error on $\widehat{P}_f$ would be larger than 0.1%. For more information on this criterion, the reader may refer to [15].

Notice finally that the value of $\varepsilon_r^{\max}$ was checked every time the surrogate model was updated except for the case where the number N_2 was too large (> 8000). The reason is related to the fact that the error computation cost is very expensive in this case. Furthermore, this cost would be with no interest since the uncertainty on the failure probability estimate is obviously significant in that case.

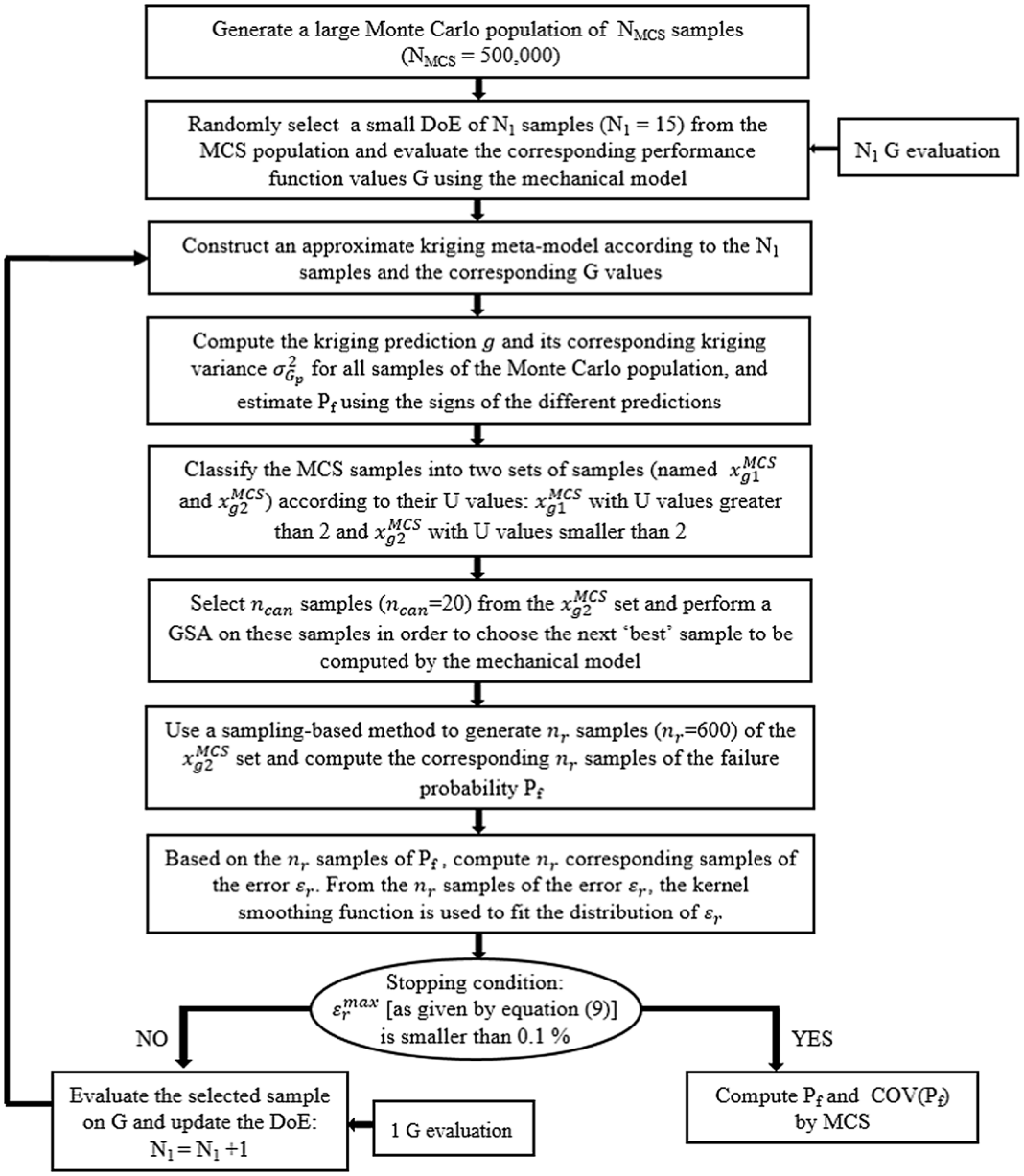

Fig. 4. Flowchart of the GSAS approach.

5. Numerical results

In this paper, the soil undrained cohesion was assumed to have a mean value that is constant with depth. A reference configuration where the soil undrained cohesion has a mean value of 50 kPa, a coefficient of variation of 10% and a vertical autocorrelation distance of 2 m was considered in the analysis. Notice however that several other values of the vertical autocorrelation distance of the soil undrained cohesion were also investigated in order to examine the effect of the vertical autocorrelation distance on the value of the failure probability.

5.1. Comparison with AK-MCS results

The implementation of AK-MCS approach for geotechnical structures involving spatially varying soil properties was recently developed by Al-Bittar et al. [40] in the case of a strip footing. Its extension to the present case of a 3D monopile foundation was performed in this paper for comparison purposes.

Fig. 5 presents the evolution of the failure probability (as given by GSAS) with the number of added samples (i.e. the samples added during the enrichment process), until reaching the stopping criterion $\varepsilon_r^{\max} < 0.1\%$. The reference configuration (a_z = 2 m) was considered in the analysis. As may be seen from this figure, the stopping condition was reached for only 44 added samples. This means that only 59 calls to the mechanical model (15 calls for the initial metamodel construction + 44 calls for the enrichment) were necessary to obtain the convergence of $\widehat{P}_f$. For this number of calls, a failure probability of 3.41×10^{-3} was obtained. The corresponding value of the error $\varepsilon_r^{\max}$ was equal to 0.08% (< 0.1%). This error was not computed before reaching 41 added samples (thus reducing the computation time) because of the high values of the uncertainty in $\widehat{P}_f$ for these cases where $N_2 > 8000$. Notice that a small value of the coefficient of variation on the failure probability was obtained [COV($\widehat{P}_f$) = 2.42%], thus indicating that the number of the generated MCS realizations (i.e. 500,000) is quite sufficient for the estimation of the failure probability using Eq. (5).

In order to check the efficiency of GSAS with respect to AK-MCS approach, a probabilistic computation has been performed on the same monopile problem but using AK-MCS approach. The failure probability

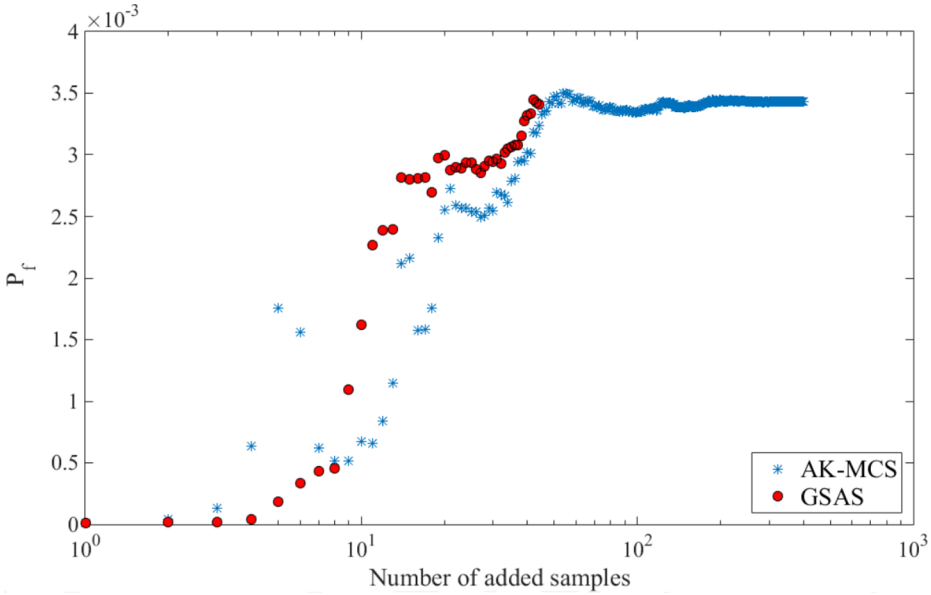

Fig. 5. Failure probability versus the number of added samples.

Table 2
Comparison of GSAS and AK-MCS results.

Method	$\hat{P}_f \times 10^{-3}$	COV($\hat{P}_f$) (%)	Number of added realizations	N_{calls}
GSAS	3.41	2.42	44	59
AK-MCS	3.41	2.42	440	455

obtained by AK-MCS was also plotted in Fig. 5 versus the number of added samples. Notice that AK-MCS computation makes use of the classical stopping criterion (i.e. Min(U) $>$ 2).

As may be seen from Fig. 5 and Table 2, GSAS is a powerful approach since it provides a quasi-similar value of the failure probability as AK-MCS making use of a much reduced number of calls to the mechanical model (59 calls in GSAS instead of 455 calls in AK-MCS). Furthermore, the obtained values of the failure probability provided by both GSAS and AK-MCS are very accurate since they correspond to a very small value of the coefficient of variation on P_f of 2.42% [see Table 2].

5.1.1. Effect of the number of added samples on the uncertainties of ε_r and P_f

This section aims at presenting the effect of the number of added samples during the enrichment process on the probability distribution of both the error ε_r and the computed failure probability.

Fig. 6 presents the distribution of ε_r for three different numbers of added samples (30 samples, 40 samples and 44 samples). The same reference configuration (a_z = 2 m) presented above was considered in the analysis. This figure shows that (i) the uncertainty of ε_r decreases with the number of added samples, the corresponding standard deviation becomes very small with a value of 2.03×10^{-4} when reaching the optimal number of added samples (i.e. 44 samples) and (ii) the final mean value of the error converges to zero. These two observations provide a quite good indication on the convergence of the estimated value of the failure probability.

Fig. 7 presents the distribution of the failure probability for three different numbers of added samples (30 samples, 40 samples and 44 samples). As in Fig. 6, one can observe a decrease in the uncertainty of this distribution with the increase in the number of added samples. A very small standard deviation value of 6.94×10^{-7} was obtained when

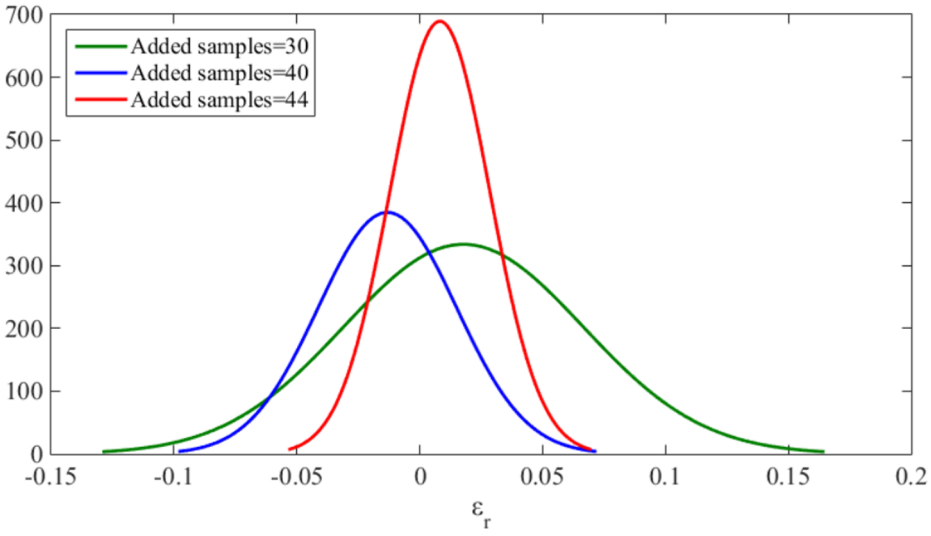

Fig. 6. Fitted distribution of ε_r for different numbers of added samples.

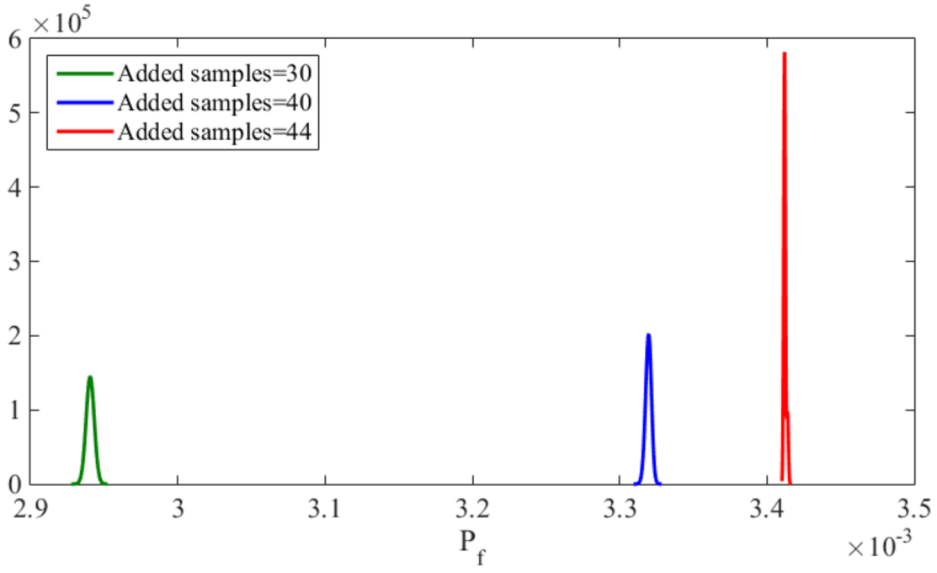

Fig. 7. Fitted distribution of the failure probability for different numbers of added samples.

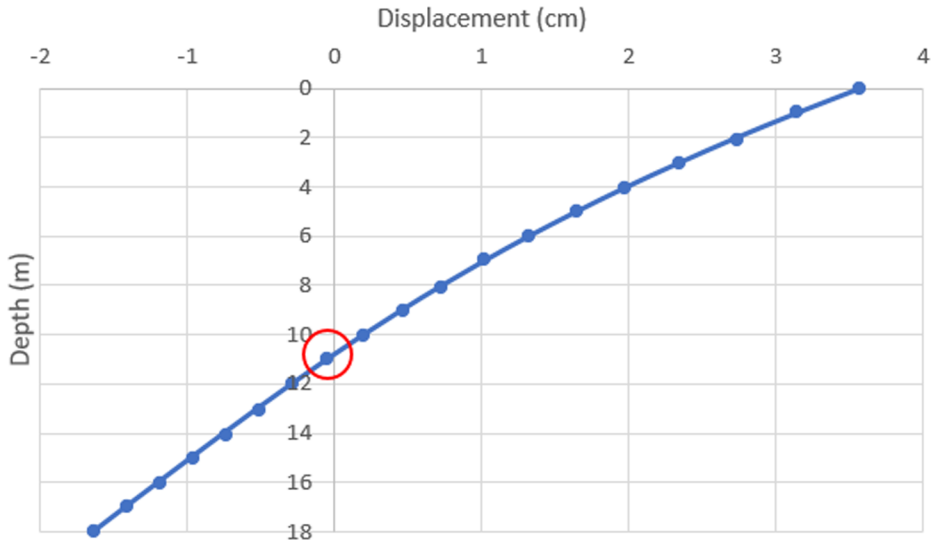

Fig. 8. Distribution of the monopile lateral displacement along the monopile embedded depth for the critical realization.

reaching the optimal number of added samples.

The obtained results confirm that the stopping criterion on the error not only makes sure that a small uncertainty on the error was reached but it also leads to a small uncertainty on the computed failure probability.

5.2. Critical and non-critical realizations

The kriging meta-model of the performance function was expressed in this paper in the standard Gaussian space of random variables. The computation of the Hasofer-Lind reliability index [43] and the corresponding design point is thus quite straightforward. A minimization of the reliability index subjected to the constraint that the performance function is equal to zero was performed. Again, the reference configuration (a_z = 2 m) presented above was considered in the analysis.

Fig. 8 shows the monopile lateral displacement versus the monopile embedded depth as obtained for the realization corresponding to the design point. A quasi-rigid behavior of the monopile can be detected with a rotation about a pivot point (indicated by a red circle in the figure) situated at a depth of about 11 m below the mudline.

Fig. 9 presents the critical realization of the soil undrained cohesion corresponding to the obtained design point. Notice that the design point corresponds to the most likely configuration to failure since it has the highest probability density among all the other points situated on the limit state surface G = 0.

Fig. 9 exhibits some symmetry in the soil cohesion about the pivot point level of the monopile. A weaker soil is observed for the depths corresponding to higher horizontal monopile displacements. It should be noted however that an increase in the value of the soil undrained cohesion was observed below the base of the monopile. This is not surprising since the soil mass under the base of the monopile has a negligible influence on the monopile horizontal displacements.

A close examination of the distribution of the undrained soil cohesion was investigated in Fig. 10. Fig. 10 (left) and (right) present respectively the distribution of the soil undrained cohesion and that of the soil displacement, along a vertical profile close to the monopile and situated in the symmetrical vertical plane at a distance of about 0.9 m in the horizontal direction.

Although a decrease in the soil cohesion was mostly observed for depths corresponding to higher horizontal displacements of the

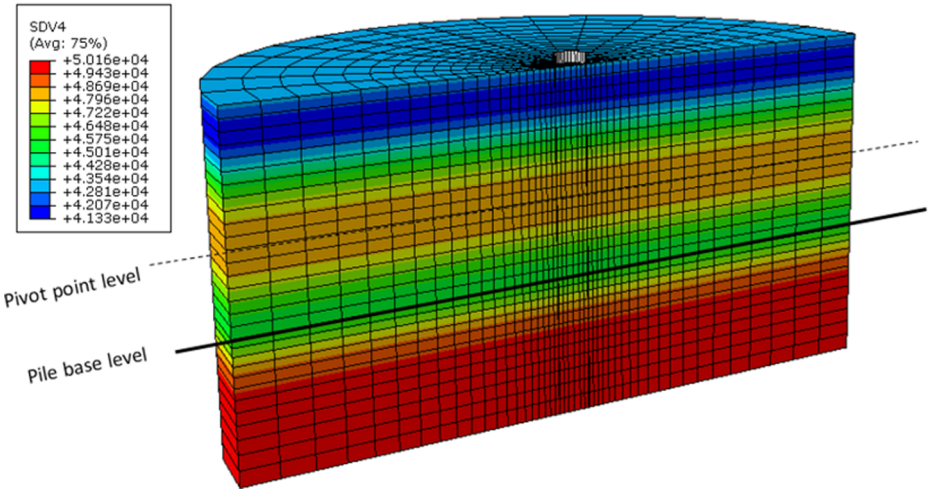

Fig. 9. Critical realization of the soil undrained cohesion.

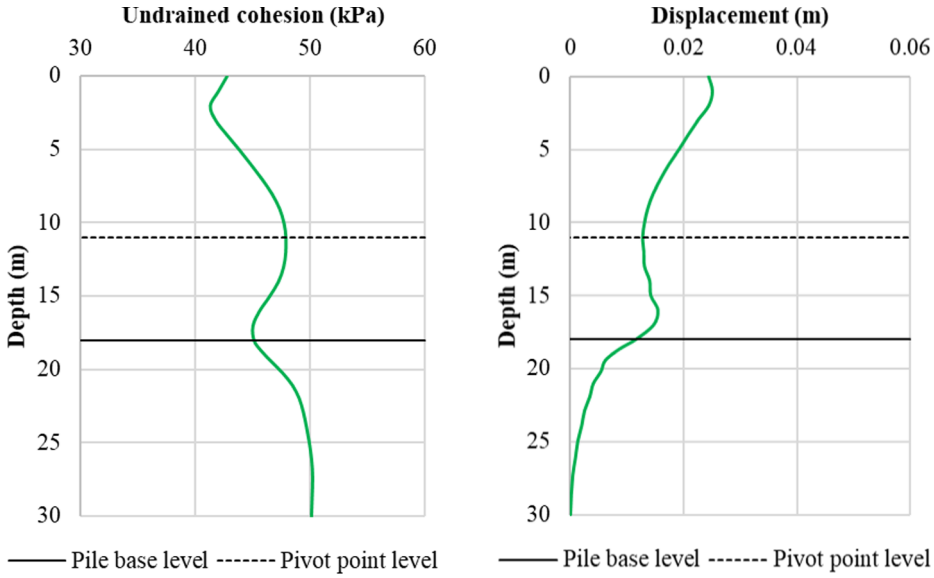

Fig. 10. Distributions of the undrained cohesion (left) and the soil displacement (right) for the critical realization.

Table 3
Adopted number of random variables and the corresponding value of the variance of error of EOLE together with the values of $\widehat{P}_f$, $COV(\widehat{P}_f)$, reliability index β_{HL} and number of added realizations for various soil variabilities.

a_z (m)	Adopted number of random variables	Variance of the error %	$\widehat{P}_f \times 10^{-3}$	COV($\widehat{P}_f$)%	β_{HL}	Number of added realizations
2	16	3.77	3.41	2.42	2.65	44
3	11	3.22	10.4	1.37	2.27	32
5	7	3.22	26.9	0.84	1.91	34
12	3	4.57	69.9	0.51	1.47	3
18	3	0.84	91.8	0.44	1.32	1
30	2	1.27	107.5	0.40	1.23	1
50	2	0.19	114.6	0.39	1.19	1
100	1	1.79	117.5	0.38	1.18	1
10,000	1	1.65×10^{-3}	120.6	0.38	1.17	1

monopile, an exception was observed in the upper zone of the monopile [see Fig. 10 (left)]. This was explained by the fact that smaller values of the soil cohesion do not correspond to higher values of the monopile horizontal displacements (as was stated above) but to higher values of the soil displacements [see Fig. 10 (right)]. Indeed, the distribution of the soil displacement (not monopile displacement) has a quasi-opposite trend to the distribution of the soil cohesion [see Fig. 10 (left) and (right)].

As a conclusion, the critical realization was found to respect not only the correlation structure of the random field (as is the case of the typical realizations) but also the mechanics of the treated problem (a smaller value of the soil cohesion was needed to induce the larger value

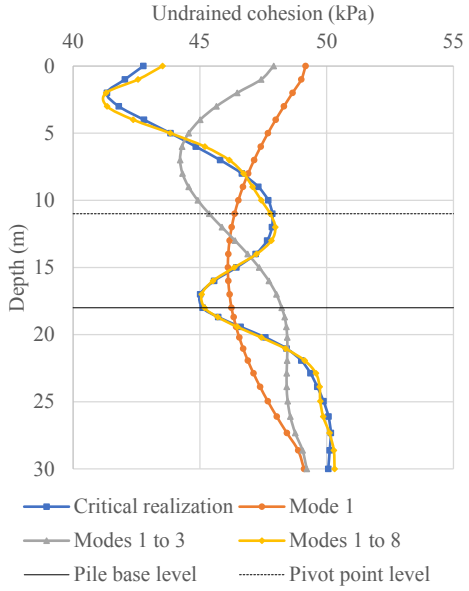

Fig. 11. Comparison between the distribution of the undrained cohesion corresponding to the critical realization and the ones corresponding to the summation of the first eigenmodes.

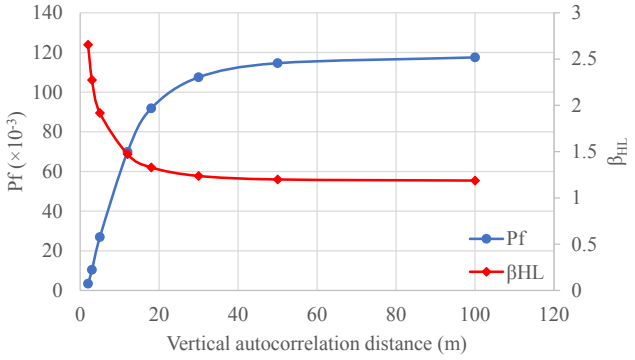

Fig. 13. Failure probability and reliability index versus the vertical autocorrelation distance.

of the soil displacement).

It should be noted that the realization of a random field is a summation of M eigenmodes. The number M of eigenmodes which was considered in the computation to arrive to a small value of the variance of error (of 3.77%) was equal to 16 [see Table 3]. Note however that only the first eight eigenmodes were influential when considering the critical realization. This number of eigenmodes is the one that is needed to globally capture the distribution of the soil cohesion (which is quasi-opposite to the soil displacement distribution) corresponding to the design point, the other eigenmodes (beyond the 8th one) being with a negligible effect on the distribution of the soil cohesion as may be seen from Fig. 11. Notice that in Fig. 11, the distribution of the cohesion was presented for only some first eigenmodes (i.e. the first single eigenmode, the first three eigenmodes and the first eight eigenmodes).

In order to visualize the distribution of the soil cohesion for the non-critical realizations and to compare them to the one corresponding to the most probable point (design point), Fig. 12 (left) shows two typical distributions of the soil cohesion corresponding to safe ($G > 0$) and unsafe ($G < 0$) zones. This figure also shows the critical distribution of the soil cohesion corresponding to the design point. As may be seen from this figure, the non-critical realizations show more fluctuations (corresponding to a higher number of influential eigenmodes) than the one corresponding to the design point. Also, they are shown not to be correlated to the soil displacements as was the case of the critical realization. Indeed, Fig. 12 (right) shows the distribution of the soil displacement for the three realizations (the one in the safe zone, the other one in the unsafe zone and that of the design point). Notice finally that all the three realizations share the following property: they respect the correlation structure of the cohesion random field.

As a conclusion, the soil displacement distribution along a vertical profile follows a quasi-similar trend for all the three realizations [cf. Fig. 12 (right)]. However, only for the critical realization case, the

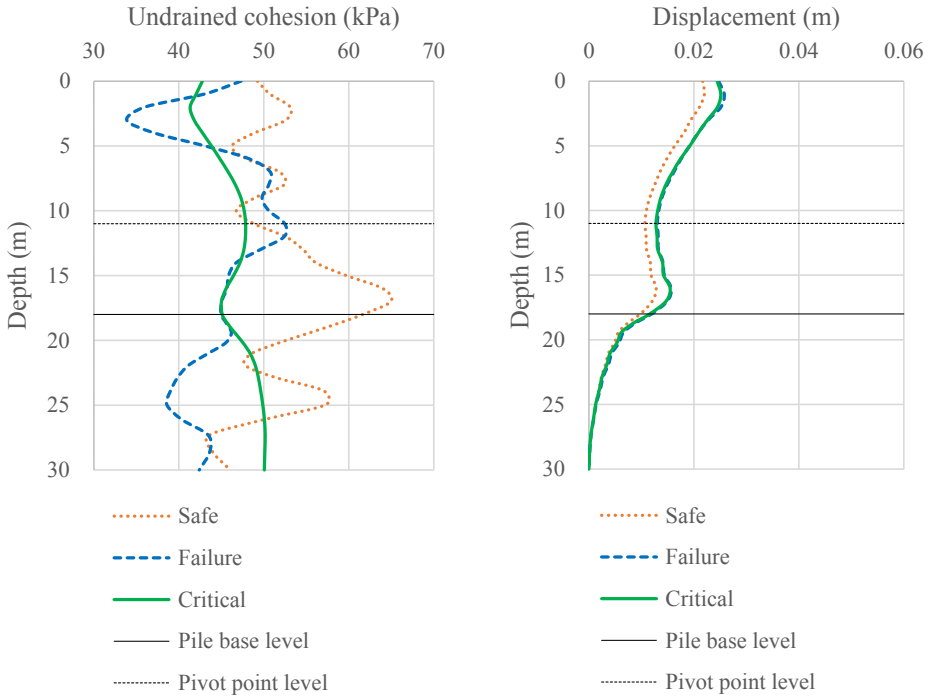

Fig. 12. Distributions of the undrained cohesion (left) and the soil displacement (right) for different realizations.

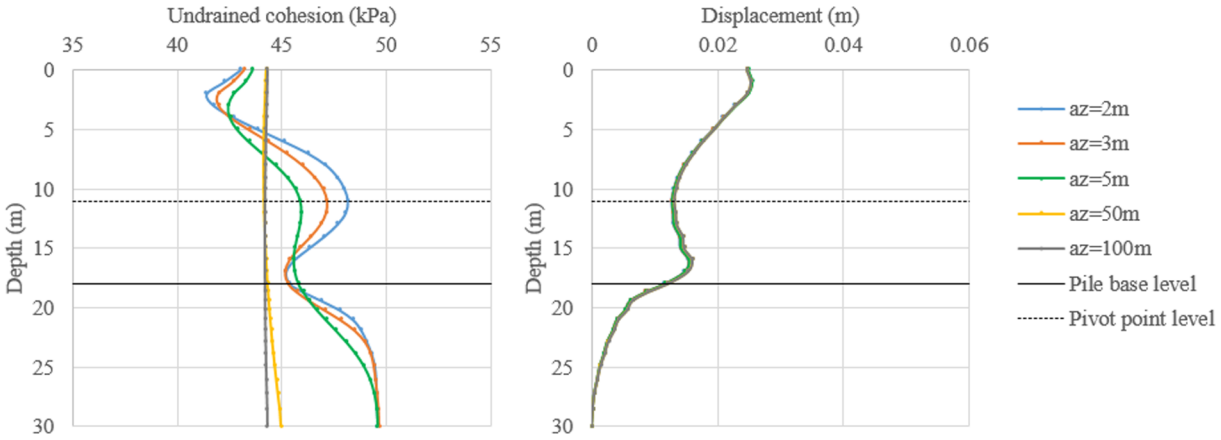

Fig. 14. Distributions of the undrained cohesion (left) and the soil displacement (right) at the critical realization for different autocorrelation distances.

cohesion distribution exhibits a quasi-opposite trend to the soil displacement distribution.

5.3. Effect of the vertical autocorrelation distance on the probabilistic outputs

The aim of this section is to investigate the effect of the vertical autocorrelation distance on the failure probability $\widehat{P}_f$ and the Hasofer-Lind reliability index β_{HL}.

Table 3 provides the number M of random variables adopted within EOLE methodology and the corresponding value of the variance of the error for different values of the vertical autocorrelation distance. As may be seen from this table, a small value of the variance of the error (smaller than 5%) was adopted for all the configurations treated in this paper. This means that a sufficiently accurate random field discretization was considered in the analysis.

As may be seen from Table 3 and Fig. 13, the failure probability increases and the Hasofer-Lind reliability index decreases with the increase in the vertical autocorrelation distance. Fig. 13 shows that the increase in the failure probability is significant for the small values of the vertical autocorrelation length (as compared to the embedded length of the monopile). Beyond the value of 18 m (length of the monopile), the increase in the failure probability becomes less significant. For the large values of the vertical autocorrelation length, the failure probability attains an asymptote corresponding to the case of a homogeneous soil.

It should be noted that the value of the coefficient of variation on the failure probability was smaller than 3% for all the configurations treated in this table. This implies that the obtained values of the failure probability are computed with accuracy. Note that the number of added realizations is small for the very large values of the vertical autocorrelation distance (case of a homogeneous soil) and it becomes larger for the small values of the vertical autocorrelation distance (i.e. for the very heterogeneous soil medium). This may be explained by the increase in the non-linearity of the meta-model for the highly heterogeneous soil. It should be emphasized that there is no regular increase in the number of added samples with the decrease in the vertical autocorrelation distance. This is because the number of added realizations depends on the evolution of the metamodel during the enrichment process.

Fig. 14 (left) shows the distributions of the undrained cohesion and Fig. 14 (right) shows the distributions of the soil displacement for different values of the vertical autocorrelation distance. These figures are provided for the critical realizations. It can be seen that the distributions of the undrained cohesion continue to follow here (for the different autocorrelation distances that are smaller than the monopile embedded depth) a quasi-opposite trend to the soil displacement. Furthermore, one can notice that the fluctuations of the soil undrained cohesion decrease with the increase of the vertical autocorrelation distance (i.e. the decrease of the soil variability) and the distribution of the soil cohesion tends to become uniform for the high values of the vertical autocorrelation distance.

6. Conclusion

A probabilistic analysis was performed at the Serviceability Limit State SLS for a large diameter monopile foundation embedded in a spatially varying clay. The soil undrained cohesion was considered as a random field following a lognormal distribution and the soil undrained Young's modulus was assumed to be linearly related to the soil undrained cohesion. EOLE method was used for the generation of realizations of the cohesion random field. The Global Sensitivity Analysis enhanced Surrogate (GSAS) modeling proposed by Hu and Mahadevan [15] was extended in this work to the case of random field and was used to perform the reliability analysis. The method has shown high efficiency as compared to AK-MCS approach since it has led to quasi similar values of the failure probability and coefficient of variation making use of a much reduced number of calls to the mechanical model.

The distribution of the soil undrained cohesion corresponding to the design point was found to follow a quasi-opposite trend to the soil displacement distribution. Smaller values of the soil cohesion were obtained for the higher values of the soil displacement. Furthermore, the critical realization depends mainly on the first few eigenmodes. These eigenmodes are those that are necessary to arrive to a cohesion distribution which has an opposite trend to the soil displacement distribution.

The failure probability was found to increase and the Hasofer-Lind reliability index was found to decrease with the increase in the vertical autocorrelation distance. The increase in the failure probability was shown significant for a ratio of monopile embedded length to the vertical autocorrelation distance bigger than 1 ($L/a_z > 1$) and tends to be negligible for the large values of the vertical autocorrelation length (as compared to the embedded length of the monopile).

Acknowledgements

This work was carried out within the framework of the WEAMEC, WEst Atlantic Marine Energy Community, and with funding from the CARENE, Communauté d'Agglomération de la Région Nazairienne et de l'Estuaire.

References

[1] Li JH, Zhou Y, Zhang LL, Tian Y, Cassidy MJ, Zhang LM. Random finite element method for spudcan foundations in spatially variable soils. Eng Geol 2016;205:146–55.
[2] Li L, Li J, Huang J, Gao F. Bearing capacity of spudcan foundations in a spatially varying clayey seabed. Ocean Eng 2017;143:97–105.
[3] Charlton TS, Rouainia M. A probabilistic approach to the ultimate capacity of skirted foundations in spatially variable clay. Struct Saf 2017;65:126–36.
[4] Vahdatirad MJ, Griffiths DV, Andersen LV, Sørensen JD, Fenton GA. Reliability analysis of a gravity-based foundation for wind turbines: a code-based design assessment. Géotechnique 2014;64:635–45.
[5] Vahdatirad MJ, Andersen LV, Ibsen LB, Clausen J, Sørensen JD. Probabilistic three-dimensional model of an offshore monopile foundation : reliability based approach. Seventh international conference on case histories in geotechnical engineering. 2013.
[6] Andersen LV, Vahdatirad MJ, Sichani MT, Sørensen JD. Natural frequencies of wind turbines on monopile foundations in clayey soils—a probabilistic approach. Comput Geotech 2012;43:1–11.
[7] Vahdatirad MJ, Andersen LV, Ibsen LB, Sørensen JD. Stochastic dynamic stiffness of a surface footing for offshore wind turbines: implementing a subset simulation method to estimate rare events. Soil Dyn Earthq Eng 2014;65:89–101.
[8] Jiang SH, Huang JS. Efficient slope reliability analysis at low-probability levels in spatially variable soils. Comput Geotech 2016;75:18–27.
[9] Li DQ, Xiao T, Cao ZJ, Zhou CB, Zhang LM. Enhancement of random finite element method in reliability analysis and risk assessment of soil slopes using subset simulation. Landslides 2016;13:293–303.
[10] Xiao T, Li DQ, Cao ZJ, Au SK, Phoon KK. Three-dimensional slope reliability and risk assessment using auxiliary random finite element method. Comput Geotech 2016;79:146–58.
[11] Huang J, Fenton G, Griffiths DV, Li DQ, Zhou CB. On the efficient estimation of small failure probability in slopes. Landslides 2017;14:491–8.
[12] Van Den Eijnden AP, Hicks MA. Efficient subset simulation for evaluating the modes of improbable slope failure. Comput Geotech 2017;88:267–80.
[13] Echard B, Gayton N, Lemaire M. AK-MCS: an active learning reliability method combining kriging and Monte Carlo simulation. Struct Saf 2011;33:145–54.
[14] Echard B, Gayton N, Lemaire M, Relun N. A combined importance sampling and kriging reliability method for small failure probabilities with time-demanding numerical models. Reliab Eng Syst Saf 2013;111:232–40.
[15] Hu Z, Mahadevan S. Global sensitivity analysis-enhanced surrogate (GSAS) modeling for reliability analysis. Struct Multidiscip Optim 2016;53:501–21.
[16] Li CC, Der Kiureghian A. Optimal discretization of random fields. J Eng Mech 1993;119:1136–54.
[17] ABAQUS. Providence: Dassault Systèmes Simulia Corp.; 2016.
[18] Recommended practice for planning, designing and constructing fixed offshore platforms—working stress design, RP2A-WSD. 21st ed. Washington: American Petroleum Institute; 2000.
[19] Kellezi L, Hansen PB. Static and dynamic analysis of an offshore mono-pile windmill foundation. BGA international conference on foundations: innovations, observations, design and practice, Dundee. 2003.
[20] Sørensen SPH, Møller M, Brødbæk KT, Augustesen AH, Ibsen LB. Numerical evaluation of load-displacement relationships for non-slender monopiles in sand. Denmark: Aalborg University; 2009. DCE technical report no. 80.
[21] Doherty P, Gavin K. Laterally loaded monopile design for offshore wind farms. Energy 2012;165:7–17.
[22] Haiderali A, Lau BH, Kenneth S, Madabhushi G. Lateral response of monopiles using centrifuge testing and finite element analysis. Phys Modell Geotech 2014;2:743–9.
[23] Briaud JL. Geotechnical engineering: unsaturated and saturated soils. Wiley; 2013.
[24] USACE. Engineering and design : settlement analysis. Engineer manual 1110–1–1904. US Army Corps of Engineers; 1990.
[25] Abaqus online documentation. Providence: Dassault systèmes simulia corp.; 2016.
[26] Jeong S, Lee J, Lee CJ. Slip effect at the pile-soil interface on dragload. Comput Geotech 2004;31:115–26.
[27] Lemos LJL, Vaughan PR. Clay-interface shear resistance. Géotechnique 2000;50:55–64.
[28] Tsubakihara Y, Kishida H. Frictional behaviour between normally consolidated clay and steel by two direct shear type apparatuses. Soils Found 1993;33:1–13.
[29] Fenton GA, Griffiths DV. Risk assessment in geotechnical engineering. Hoboken (NJ): Wiley; 2008.
[30] Al-bittar T, Soubra AH. Bearing capacity of strip footings on spatially random soils using sparse polynomial chaos expansion. Int J Numer Anal Meth Geomech 2013;37:2039–60.
[31] Li DQ, Xiao T, Cao ZJ, Phoon KK, Zhou CB. Efficient and consistent reliability analysis of soil slope stability using both limit equilibrium analysis and finite element analysis. Appl Math Model 2016;40:5216–29.
[32] Xiao T, Li DQ, Cao ZJ, Tang XS. Full probabilistic design of slopes in spatially variable soils using simplified reliability analysis method. Georisk: Assess Manage Risk Eng Syst Geohazards 2017;11:146–59.
[33] Vanmarcke EH. Random fields: analysis and synthesis: revised and expanded. new ed. Singapore: World Scientific Publishing; 2010.
[34] Vanmarcke EH. Probabilistic modeling of soil profiles. J Geotech Eng 1977;103:1227–46.
[35] Lacasse S, Nadim F. Uncertainties in characterising soil properties. In: Shackelford CD, Nelson PP, Roth MJS, editors. Proceedings of uncertainty in the geologic environment: from theory to practice. Geotechnical Special Publication (GSP 58), ASCE; 1996. p. 49–75.
[36] Al-bittar T, Soubra AH. Probabilistic analysis of strip footings resting on spatially varying soils and subjected to vertical or inclined loads. J Geotech Geoenviron Eng, ASCE 2014;140.
[37] Clausen J, Damkilde L, Andersen L. An efficient return algorithm for non-associated plasticity with linear yield criteria in principal stress space. Comput Struct 2007;85:1795–807.
[38] Papazafeiropoulos G, Muñiz-calvente M, Martínez-pañeda E. Abaqus2Matlab: a suitable tool for finite element post-processing. Adv Eng Softw 2017;105:9–16.
[39] Sacks J, Welch WJ, Mitchell TJ, Wynn HP. Design and analysis of computer experiments. Stat Sci 1989;4:409–23.
[40] Al-bittar T, Soubra AH, Thajeel J. Kriging-based reliability analysis of strip footings resting on spatially varying soils. J Geotech Geoenviron Eng, ASCE 2018;144.
[41] Lophaven SN, Nielsen HB, Søndergaard J. DACE: A matlab kriging toolbox version 2.0. Informatics and mathematical modelling. Technical University of Denmark, DTU; 2002. Technical report IMM-TR-2002-12.
[42] Xu C, Gertner G. Extending a global sensitivity analysis technique to models with correlated parameters. Comput Stat Data Anal 2007;51:5579–90.
[43] Hasofer AM, Lind MC. An exact and invariant second-moment code format. J Eng Mech 1974;100:111–21.